Nickel-Catalyzed Asymmetric Alkene Hydrogenation of α,β-Unsaturated Esters: High-Throughput Experimentation-Enabled Reaction Discovery, Optimization, and Mechanistic Elucidation

Michael Shevlin,*,[†] Max R. Friedfeld,[‡] Huaming Sheng,[†] Nicholas A. Pierson,[†] Jordan M. Hoyt,[‡] Louis-Charles Campeau,[†] and Paul J. Chirik*,[‡]

[†]Department of Process & Analytical Chemistry, Merck & Co., Inc., Rahway, New Jersey 07065, United States
[‡]Department of Chemistry, Princeton University, Princeton, New Jersey 08544, United States

Ⓢ *Supporting Information*

ABSTRACT: A highly active and enantioselective phosphine-nickel catalyst for the asymmetric hydrogenation of α,β-unsaturated esters has been discovered. The coordination chemistry and catalytic behavior of nickel halide, acetate, and mixed halide-acetate with chiral bidentate phosphines have been explored and deuterium labeling studies, the method of continuous variation, nonlinear studies, and kinetic measurements have provided mechanistic understanding. Activation of molecular hydrogen by a trimeric $(Me-DuPhos)_3Ni_3(OAc)_5I$ complex was established as turnover limiting followed by rapid conjugate addition of a nickel hydride and nonselective protonation to release the substrate. In addition to reaction discovery and optimization, the previously unreported utility high-throughput experimentation for mechanistic elucidation is also described.
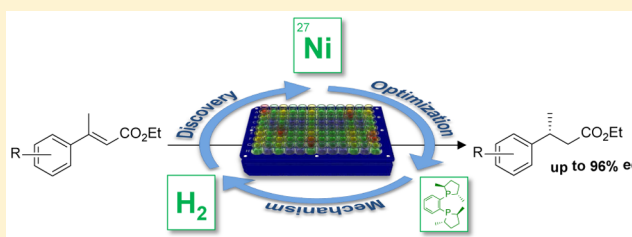
INTRODUCTION

Enantiopure chiral compounds are important molecular agents for the treatment of disease. Indeed, of the 29 small molecules approved by the United States Food and Drug Administration in 2014, 22 were chiral.[1] The synthesis of chiral compounds by metal-catalyzed asymmetric hydrogenation is a powerful synthetic method employed on an industrial scale for the synthesis of pharmaceuticals,[2] agrochemicals,[3] flavors and fragrances,[4] and fine chemicals.[5] However, most asymmetric hydrogenation methods rely on precious metal catalysts based on rhodium, ruthenium, or iridium[6] and suffer from their associated high costs and deleterious environmental impact. By contrast, catalysts containing first-row transition elements offer potential advantages in cost, sustainability, and the possibility of new chemistry derived from substitutional lability. Recently, the cobalt-catalyzed asymmetric hydrogenation of C=C bonds[7] and the iron-catalyzed asymmetric hydrogenation of C=O and C=N bonds[8] have been reported. While these reports demonstrate the potential of first-row transition elements in asymmetric hydrogenation and overcome challenges associated with precious metal catalysts, significant catalyst development is required before first-row transition metals can rival the reactivity, substrate scope, and ease of handling typically associated with rhodium, ruthenium, and iridium asymmetric hydrogenation catalysts. As part of these objectives, nickel catalysts for asymmetric alkene hydrogenation were explored.

While heterogeneous nickel catalysts have a long-standing history and maintain a prominent role in reduction reactions including hydrogenation of olefins,[9] there are scant reports of homogeneous nickel hydrogenation catalysts.[10] The facility and speed with which homogeneous systems can be tuned for reactivity and selectivity by ligand alteration makes them attractive avenues for the development of enantioselective hydrogenation catalysts on various substrate classes. In an ideal case, such a system could activate molecular hydrogen, which is an inexpensive, readily available, and atom economical reagent that produces no waste.

While asymmetric reduction of ketones promoted by nickel catalysts using H_2 gas has recently been reported, no mechanistic insight into the mechanism of hydrogen activation or mode of stereoinduction have been described.[11] Given this limited precedent, it is not surprising that there are still no examples of asymmetric reductions of olefins using chiral homogeneous nickel catalysts with H_2 gas. Only nickel-catalyzed enantioselective transfer hydrogenation of olefins using formic acid and triethylamine as a reductant has recently appeared.[12] Herein we describe the discovery of the first homogeneous nickel-catalyzed asymmetric hydrogenation of α,β-unsaturated esters, using H_2 gas as the terminal reductant, in high yield and high enantioselectivity of the products. Catalyst discovery, optimization, and in-depth mechanistic studies were enabled by high throughput experimentation (HTE) allowing identification of a unique phosphine-ligated trimetallic mixed carboxylate halide nickel complex as the active
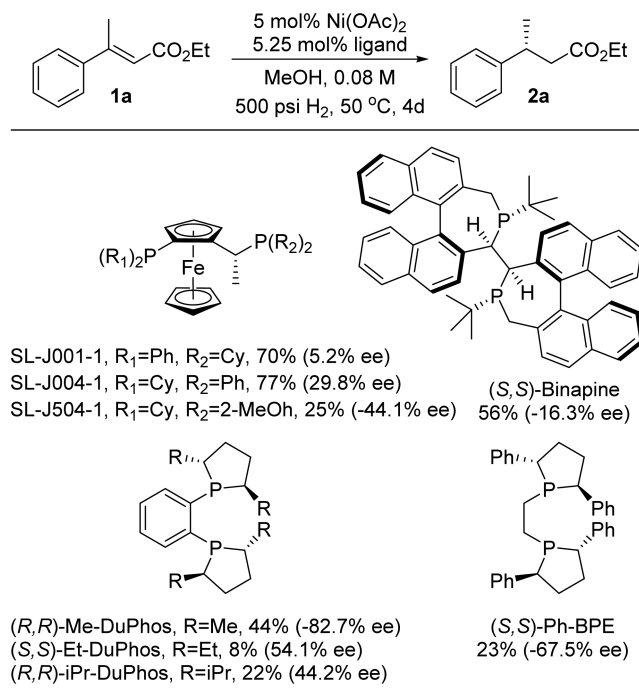
catalyst for heterolytic dihydrogen activation and alkene hydrogenation.

RESULTS

Catalyst Discovery and Optimization. Ethyl β-methylcinnamate (**1a**) was selected as a representative substrate given that the products of hydrogenation, chiral dihydrocinnamates, are important motifs in pharmaceuticals,[13] odorants,[14] natural products,[15] and synthetic intermediates[16] and are often challenging substrates for many asymmetric hydrogenation catalysts due to the relatively poor ability of the ester to function as a directing group. On the basis of the success of nickel(II)−phosphine complexes in the hydrogenation of primary alkenes,[10] we reasoned similar enantiopure variants of these catalysts may be effective for the asymmetric hydrogenation of α,β-unsaturated esters. HTE is a powerful technique for rapidly conducting large arrays of experiments and was used to facilitate the discovery of nickel hydrogenation catalysts.[17]

A library of 192 chiral bidentate phosphine ligands combined with Ni(OAc)$_2$ was examined for the hydrogenation of **1a** in methanol solution at 500 psi of H$_2$ at 50 °C (Scheme 1). While

Scheme 1. Selected Results of the Evaluation of Enantiopure Bis(phosphines) with Ni(OAc)$_2$ for the Asymmetric Hydrogenation of 1a[a]

SL-J001-1, R$_1$=Ph, R$_2$=Cy, 70% (5.2% ee)
SL-J004-1, R$_1$=Cy, R$_2$=Ph, 77% (29.8% ee)
SL-J504-1, R$_1$=Cy, R$_2$=2-MeOh, 25% (−44.1% ee)

(S,S)-Binapine
56% (−16.3% ee)

(R,R)-Me-DuPhos, R=Me, 44% (−82.7% ee)
(S,S)-Et-DuPhos, R=Et, 8% (54.1% ee)
(R,R)-iPr-DuPhos, R=iPr, 22% (44.2% ee)

(S,S)-Ph-BPE
23% (−67.5% ee)

[a]Results are reported as conversion (% ee) as determined by chiral reverse phase HPLC. Reactions favoring (R)-**2a** are denoted with positive values of % ee while reactions favoring (S)-**2a** are denoted with negative values of % ee.

cyclohexyl-substituted Josiphos ligands[18] provided good reactivity, the enantioselectivities were modest. Likewise, Binapine[19] resulted in moderate conversion with low enantioselectivity. Bis(phospholane) ligands in the DuPhos and BPE families[20] produced low reactivity but yielded encouraging enantioselectivity; the best result was with Me−DuPhos with 82.7% ee at 44% conversion.

Various nickel precursors and additives were next evaluated to improve catalyst performance. Each experiment was conducted with Me−DuPhos as the chiral phosphine with **1a** as the substrate. These experiments uncovered a remarkable complementary effect between with mixed halide−acetate nickel combinations (Table 1).[21] While nickel halides alone in combination with Me−DuPhos produced low reactivity and selectivity, addition of Bu$_4$NOAc or, conversely, Ni(OAc)$_2$ mixed with tetrabutylammonium halides increased both reactivity and enantioselectivity. The order of increasing reactivity and enantioselectivity was found to be Cl < Br < I, and both NiI$_2$/Bu$_4$NOAc and Ni(OAc)$_2$/Bu$_4$NI afforded complete conversion to the product in 94.3% ee.[22]

Having improved the reactivity and selectivity of the catalyst, various reaction parameters were optimized (Table 2). The loading of the nickel precursor was reduced from 5 to 2 mol % and complete conversion was maintained (entries 1 and 2), while additional iodide additive produced lower reactivity (entry 3).[23] Evaluation of the hydrogenation reaction in various solvents established methanol as optimal (entries 4−10). Increasing the concentration of the catalytic reaction to 0.5 M resulted in maximum reactivity (entries 11−15) and addition of 10% (by volume) of water to the hydrogenation had minimal impact on performance (entry 13), a significant advance in catalysis with Earth abundant transition metals. At temperatures below 50 °C, turnover was minimal (entry 16) while increasing the temperature to 80 °C maintained reactivity but eroded enantioselectivity (entry 17). Increasing the hydrogen pressure to 1500 psi allowed a reduction in nickel loading to 0.5 mol % (entries 18 and 19). Subsequent experiments were conducted at 500 psi of H$_2$ and 1 mol % Ni precursor for ease of handling and to obtain complete conversion in convenient reaction times (entry 20). Decreasing reaction pressure did confer a small enantioselectivity benefit, but with significantly lower reactivity (entries 21 and 22).

With optimized reaction conditions in hand, the scope of the asymmetric hydrogenation was examined (Table 3). Both electron-rich (entries 2−4) and electron-poor (entries 5 and 6) substrates were hydrogenated with excellent enantioselectivity; the electron poor alkenes exhibited slightly lower reactivity. Potentially coordinating functional groups containing nitrogen atoms (entries 3 and 7) and thioethers (entry 4) were well tolerated. Introduction of an ortho methyl substituent in the phenyl ring resulted in lower reactivity and enantioselectivity likely due to crowding of the alkene (entry 8). In contrast to previous reports in nickel-catalyzed transfer hydrogenation with formic acid-triethylamine,[12] aryl chlorides and bromides were well-tolerated, with only small amounts of protodehalogenation detected (entries 9 and 10). The phenylated butenolide substrate, **1k**, was also well tolerated (entry 11).

Coordination Chemistry. Having identified the optimal catalytic conditions, synthesis and characterization of a well-defined nickel precatalyst was explored. Previous work from our laboratory[7a] has demonstrated the superior performance of isolated precatalysts over analogous compounds generated in situ. Stirring a THF solution of (S,S)-Me−DuPhos with a methanol solution of Ni(OAc)$_2$·4H$_2$O at 50 °C for 30 min followed by filtration and recrystallization resulted in isolation of ((S,S)-Me−DuPhos)Ni(OAc)$_2$ as an air-stable yellow solid. The chloroform-d ^{1}H NMR spectrum exhibits the number of peaks consistent with a C$_2$ symmetric compound. A broad singlet was also observed in the ^{31}P NMR spectrum and is also consistent with a fluxional, C$_2$-symmetric compound where the

Table 1. Nickel Precursor and Additive Effects in the Enantioselective Hydrogenation of Substrate 1a with Me−DuPhos as the Enantiopure Bis(phosphine).[a]

5 mol% NiY$_2$
5.25 mol% (S,S)-Me-DuPhos
10% Bu$_4$NX
MeOH, 0.2 M
500 psi H$_2$, 50 °C, 18 h

	Bu$_4$NX additive				
NiY$_2$ source	none	Bu$_4$NCl	Bu$_4$NBr	Bu$_4$NI	Bu$_4$NOAc
NiCl$_2$	0.0	0.0	0.2	0.7	35 (90.1)
NiBr$_2$	1.3	0.3	0.2	0.4	98 (92.1)
NiI$_2$	1.3	0.4	0.4	0.4	100 (94.4)
Ni(OAc)$_2$	33 (64.1)	23 (90.5)	88 (93.5)	100 (94.3)	19 (67.5)

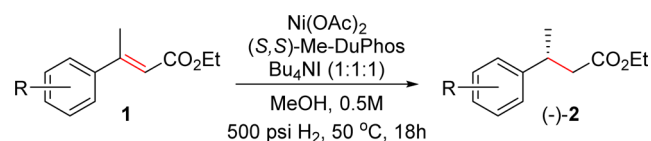[a]Results are reported as conversion (% ee) as determined by chiral reverse phase HPLC.

Table 2. Optimization of Reaction Parameters in the Nickel-Catalyzed Asymmetric Hydrogenation of 1a
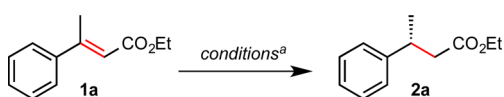
entry	mol % Ni	solvent	conc. (M)	press. (psi)	temp. (°C)	conv.[b]	%ee[b]
1	5	MeOH	0.2	500	50	100	94.2
2	2	MeOH	0.2	500	50	99	93.7
3	2[c]	MeOH	0.2	500	50	68.3	95.1
4	2	EtOH	0.2	500	50	93	94.5
5	2	iPrOH	0.2	500	50	69.7	94
6	2	TFE	0.2	500	50	100	38
7	2	THF	0.2	500	50	21.7	94
8	2	PhMe	0.2	500	50	33.2	89
9	2	PhCF$_3$	0.2	500	50	85.4	95.4
10	2	MeCN	0.2	500	50	16.8	95.5
11	0.5	MeOH	0.2	500	50	10.3	93
12	0.5	MeOH	0.5	500	50	62.9	94.6
13	0.5	MeOH[d]	0.5	500	50	70.2	94.2
14	0.5	MeOH	1	500	50	49.3	95.2
15	0.5	neat	5.5	500	50	10	95.1
16	0.5	MeOH	0.5	500	20	0.5	-
17	0.5	MeOH	0.5	500	80	100	88.9
18	0.5	MeOH	0.5	1000	50	93.5	94
19	0.5	MeOH	0.5	1500	50	99.3	93.7
20	1	MeOH	0.5	500	50	100	94.8
21	1	MeOH	0.5	300	50	53.9	95.8
22	1	MeOH	0.5	100	50	16.5	96.1

[a]Ni(OAc)$_2$: (S,S)-Me−DuPhos: Bu$_4$NI (1:1.05:1), 18h. [b]Conversion and %ee determined by chiral reverse phase HPLC. [c]2:1 Bu$_4$NI: Ni used. [d]10 vol % water added.

Table 3. Enantioselective Hydrogenation of α,β-Unsaturated Esters[a]

Ni(OAc)$_2$
(S,S)-Me-DuPhos
Bu$_4$NI (1:1:1)
MeOH, 0.5M
500 psi H$_2$, 50 °C, 18h

Entry	Product	Entry	Product
1	(-)-2a — 1% Ni, 99%, 93.0% ee	2	(-)-2b — 1% Ni, 97%, 94.7% ee
3	(-)-2c — 1% Ni, 97%, 86.5% ee	4	(-)-2d — 1% Ni, 98%, 95.6% ee
5	(-)-2e — 2% Ni, 87%, 95.5% ee	6	(-)-2f — 3% Ni, 90%, 92.7% ee[b]
7	(-)-2g — 5% Ni, 92%, 72.7% ee[c]	8	(-)-2h — 5% Ni, 85%, 77.6% ee[d]
9	(-)-2i — 2% Ni, 87%, 94.6% ee	10	(-)-2j — 2% Ni, 94%, 94.1% ee[e]
11	(-)-2k — 1% Ni, 97%, 82.0% ee		

[a]Isolated yield and %ee reported. Unless noted, all reactions reached >98% conversion to alkane. Conversion and %ee determined by chiral reverse phase HPLC or chiral SFC. [b]96% conversion. [c]98% conversion. [d]94% conversion. [e]97% conversion, 1.4% of 2a formed.

dynamic behavior likely arises from $\kappa^2-\kappa^1$ interconversion of the acetate ligands. Cooling a concentrated fluorobenzene solution of ((S,S)-Me−DuPhos)Ni(OAc)$_2$ to −35 °C produced single crystals suitable for X-ray diffraction. The solid state structure of ((S,S)-Me−DuPhos)Ni(OAc)$_2$ established an idealized planar Ni(II) center, where the carbonyl oxygen of each acetate ligand is oriented toward, but not discretely bound to, the nickel center (Ni—O$_{carbonyl}$ bond distances = 2.847 and 3.010 Å).

The coordination chemistry of the nickel halide precursor proved more complicated. The solid-state structure of previously reported ((S,S)-Me−DuPhos)NiI$_2$[24] was confirmed

using single crystals obtained from mixing a 1:1 ratio of (S,S)-Me−DuPhos and solid NiI$_2$ in THF/methanol followed by recrystallization. Notably, the ^{1}H-, ^{13}C-, and ^{31}P-NMR spectra of this mixture were inconsistent with the expected C$_2$-

symmetric compound. Instead the chloroform-*d* ^{31}P-NMR spectrum exhibited a 1:1 ratio of two higher order multiplets (see SI for details) consistent with coordination of *two* inequivalent (*S,S*)-Me−DuPhos chelates. The spectroscopic data are most consistent with $[((S,S)\text{-Me−DuPhos})_2\text{NiI}][\text{I}]$ as the species formed in highest concentration where the two phosphine ligands and one iodide ligand define the pseudotrigonal bipyramidal geometry about the nickel with an outer sphere iodide anion. The inner-sphere iodide ligand completes the equatorial plane. While the maximum in situ NMR yield of $[((S,S)\text{-Me−DuPhos})_2\text{NiI}][\text{I}]$ was obtained at a 2:1 ratio of phosphine to NiI_2, detectable quantities (∼1−3%) of $((S,S)\text{-Me−DuPhos})\text{NiI}_2$ were observed. Five coordinate $[((S,S)\text{-Me−DuPhos})_2\text{NiI}][\text{I}]$ was inactive for the hydrogenation of **1a** under standard conditions. Controlling the metal−ligand ratios (1:1 or 1:2) using stock solutions of NiI_2 in methanol resulted in the reliable synthesis of either $((S,S)\text{-Me−DuPhos})\text{NiI}_2$ or $[((S,S)\text{-Me−DuPhos})_2\text{NiI}][\text{I}]$ (see SI for details). Interconversion between these two complexes was demonstrated by adding additional NiI_2 solution to a CDCl_3 solution of $[((S,S)\text{-Me−DuPhos})_2\text{NiI}][\text{I}]$ at room temperature, resulting in partial conversion to $((S,S)\text{-Me−DuPhos})\text{NiI}_2$.

Attempts to prepare and isolate $((S,S)\text{-Me−DuPhos})\text{Ni(OAc)I}$ have been unsuccessful. While broadened ^{1}H and ^{31}P NMR signals were observed upon addition of various iodide sources to $((S,S)\text{-Me−DuPhos})\text{Ni(OAc)}_2$, attempts to isolate a new product repeatedly resulted in crystallization of $((S,S)\text{-Me−DuPhos})\text{NiI}_2$.[24] Mass spectrometry studies following addition of NaI to a methanol solution of $((S,S)\text{-Me−DuPhos})\text{Ni(OAc)}_2$ revealed a mixture of monomeric, dimeric, and trimeric nickel complexes containing acetate and iodide ancillary ligands. All of the complexes detected by MS were either cationic or sodium adducts of neutral complexes; no anionic nickel species were detected in negative ion mode.

Determination of Catalyst Stoichiometry by the Method of Continuous Variation. Because of the challenges associated with isolation of well-defined, catalytically relevant intermediates, alternative characterization methods were employed in an attempt to identify the active nickel species responsible for the enantioselective hydrogenation of **1a**. The method of continuous variation ("Job plots") was used to elucidate catalyst stoichiometry.[25] Rather than measure a property of the catalyst (or more likely a catalyst resting state) directly, catalytic performance as a function of a range of precursor component ratios were evaluated. The method of continuous variation is applicable when all conditions examined do not result in complete conversion to product; thus, conditions were used that produced partial conversion for all stoichiometries examined. The ability of HTE to execute arrays of reactions under identical conditions proved critical for the rapid completion of these experiments. While it is conceivable that a single multidimensional Job plot[26] would reveal the stoichiometry of nickel and its three potential ligands (Me−DuPhos, acetate, iodide), we hypothesized that the same information could also be gleaned from a series of conventional Job plots by fixing the stoichiometry of some species relative to each other while varying their mole fraction against others. This approach would require far fewer reactions and provide higher resolution data. The results of these studies are presented in Figure 1.

Conditions **C1** and **C3** fixed the stoichiometries of Ni(OAc)_2 with $^n\text{Bu}_4\text{NI}$ and NiI_2 with $^n\text{Bu}_4\text{NOAc}$, respectively, and varied their mole fraction versus (*S,S*)-Me−DuPhos. Both of these
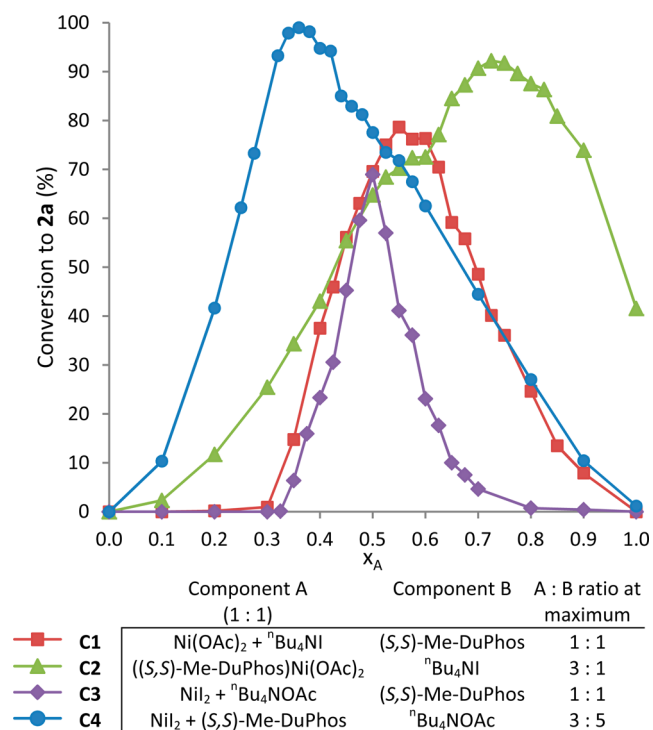

	Component A (1 : 1)	Component B	A : B ratio at maximum
C1	$\text{Ni(OAc)}_2 + {}^n\text{Bu}_4\text{NI}$	(*S,S*)-Me-DuPhos	1 : 1
C2	$((S,S)\text{-Me-DuPhos})\text{Ni(OAc)}_2$	$^n\text{Bu}_4\text{NI}$	3 : 1
C3	$\text{NiI}_2 + {}^n\text{Bu}_4\text{NOAc}$	(*S,S*)-Me-DuPhos	1 : 1
C4	$\text{NiI}_2 + (S,S)\text{-Me-DuPhos}$	$^n\text{Bu}_4\text{NOAc}$	3 : 5

Figure 1. Job plots for asymmetric hydrogenation of **1a**. *Conditions:* 50 μmol (9.5 mg) scale, MeOH, 0.5M, 500 psi H_2, 50 °C, 18h.

conditions yielded maximum conversion to product at a mole fraction of 0.5, indicating a 1:1 Ni/DuPhos stoichiometry. Condition **C2** fixed the Ni(OAc)_2 and (*S,S*)-Me−DuPhos stoichiometry and varied their mole fraction versus $^n\text{Bu}_4\text{NI}$; maximum conversion at a mole fraction of 0.75 and indicates 3:1 Ni/I stoichiometry. Finally, condition **C4** fixed NiI_2 and (*S,S*)-Me−DuPhos stoichiometry and varied their mole fraction versus $^n\text{Bu}_4\text{NOAc}$; maximum conversion at a mole fraction of 0.36, suggesting either a 1:2 Ni/OAc stoichiometry ($x = 0.33$) or a 3:5 Ni/OAc stoichiometry ($x = 0.375$). Combined with the MS studies that indicate an absence of anionic nickel complexes, these experiments are consistent with a catalyst stoichiometry of $((S,S)\text{-Me−DuPhos})_3\text{Ni}_3(\text{OAc})_5\text{I}$.[27] This stoichiometry is likely associated with a resting state and corresponds to conditions designed to obtain optimal conversion and does not represent a true active catalyst. As will be described in a subsequent section, reaction with H_2 is rate determining, and the resulting nickel hydride responsible for alkene insertion have a different stoichiometry than $((S,S)\text{-Me−DuPhos})_3\text{Ni}_3(\text{OAc})_5\text{I}$. It also should be noted that shoulders are observed in the data with **C2** and **C3** and are consistent with formation of multiple species under catalytic conditions that are likely interconverting on the time scale of the catalytic reaction. These observations are also consistent with the low activity of the simple $((S,S)\text{-Me−DuPhos})\text{NiX}_2$ compounds.

The presence of a trimetallic nickel species under catalytic conditions suggested that nonlinear effects would also be likely. As shown in Figure 2, a negative nonlinear effect was observed upon mixing compositions of Me−DuPhos with varying enantiopurity. Least squares curve fitting support a trimeric $(\text{ML})_3$ system with a statistical distribution of ligands, with $g = r_{\text{heterochiral}}/r_{\text{homochiral}} = 1.16$ and $\text{ee}_0' = 6.05\%$, indicating a heterochiral catalyst with slightly higher reactivity and lower selectivity compared to the homochiral catalyst.[28]

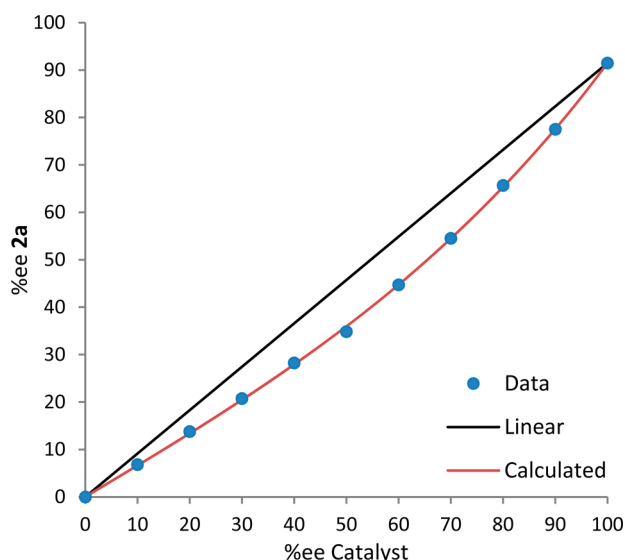**Figure 2.** Nonlinear study for asymmetric hydrogenation of **1a**. *Conditions:* 20 μmol (3.8) mg scale, 1% Ni(OAc)$_2$/Bu$_4$NI/Me–DuPhos (1:1:1.05), MeOH, 0.2 M, 500 psi H$_2$, 50 °C, 18 h.

Mechanistic Studies. With insight into the nature of the active species formed under catalytic hydrogenation conditions, the order of the catalytic reaction with respect to each of the components was determined. Such information is critical for determining the stoichiometry of the transition structure in the turnover-limiting step of the catalytic reaction. The successful application of microscale HTE to Job plots and nonlinear studies motivated use of similar techniques for kinetic analyses. By conducting catalyst-loading studies under conditions selected to produce partial conversion across the data set, the manner in which conversion varied with catalyst loading would yield the rate law. Assuming the concentration of catalyst does not change over time, the differential rate law can be expressed as follows:

$$-\frac{d[S]}{dt} = k[\text{Cat}]^a[\text{H}_2]^b[S]^c \tag{1}$$

where $[S]$ and $[\text{Cat}]$ are the substrate and catalyst concentrations and a, b, and c are the order of the reaction with respect to catalyst, hydrogen, and substrate, respectively. Separation of terms and integration yields:

$$-\int_{[S]_0}^{[S]_t} \frac{1}{[S]^c}\, d[S] = \int_0^t k[\text{Cat}]^a[\text{H}_2]^b\, dt \tag{2}$$

This expression can be solved for various reactions orders c with respect to the substrate to provide familiar integrated rate laws. For example, for a reaction that is zero order in substrate with constant catalyst and hydrogen concentration,

$$[S]_t = -k[\text{Cat}]^a[\text{H}_2]^b t + [S]_0 \tag{3}$$

Likewise, for reactions that are first and second order with respect to substrate, these integrated rate laws, respectively, are as follows:

$$\ln[S]_t = -k[\text{Cat}]^a[\text{H}_2]^b t + \ln[S]_0 \tag{4}$$

$$\frac{1}{[S]_t} = k[\text{Cat}]^a[\text{H}_2]^b t + \frac{1}{[S]_0} \tag{5}$$

Traditionally, a plot of $[S]$, $\ln\,[S]$, or $1/[S]$ vs time is prepared, and reaction order is established by linearity. We hypothesized that if $[\text{Cat}]^a$ or $[\text{H}_2]^b$ were instead plotted as the independent variable while holding time constant, then similar conclusions about the order of the reaction would be able to be drawn, not only about the order of the reaction with respect to the substrate, but also with respect to catalyst and H$_2$.

For this transformation, plots of **1a** remaining versus catalyst concentration at different H$_2$ pressures are linear (Figure 3),
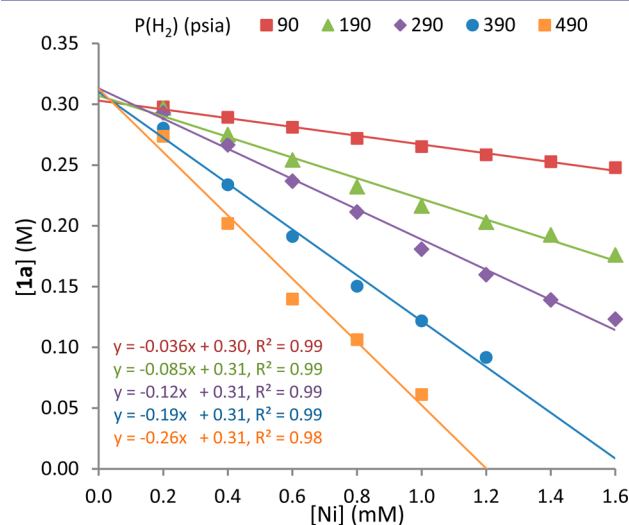

Figure 3. Plot of **1a** remaining vs catalyst concentration for the asymmetric hydrogenation of **2a**. *Conditions:* 30 μmol (5.7 mg) scale, Ni(OAc)$_2$/(S,S)-Me–DuPhos/Bu$_4$NI (1:1:1), MeOH, 0.3 M, 90–490 psia H$_2$, 50 °C, and 19.25h.

suggesting that the reaction is zero order with respect to substrate and first order with respect to nickel species.[29] Likewise, plots of **1a** remaining versus H$_2$ pressure for different catalyst concentrations are linear (Figure 4), suggesting the reaction is first order in hydrogen. These results were confirmed on gram scale by hydrogen uptake and with in situ IR measurements.

With the kinetic data in hand, a series of additional experiments were conducted to gain insight into the mechanism of action. Open questions include the role of the acetate ligands in the H$_2$ activation process and what redox processes, if any, at nickel are operative. Such insights are critical for rational design of next generation catalysts with improved performance. A series of isotopic labeling studies was conducted; the first of which involved the reduction of **1a** with 500 psi of D$_2$ gas in CH$_3$OH solution. Analysis of the **2a** produced from this reaction established exclusive formation of the d_1 isotopologue where the deuterium label was incorporated solely at the benzylic position of the alkane (Scheme 2a). Repeating the experiment with H$_2$ gas and CH$_3$OD produced a different isotopomer of **2a**-d_1, where the deuterium was located as an approximately 1:1 ratio in the diastereotopic positions adjacent to the ester functional group (Scheme 2b). Performing the hydrogenation reaction with both D$_2$ and CH$_3$OD yielded the expected **2a**-d_2 product (Scheme 2c) where deuterium was located in the benzylic position and on the carbon adjacent to the ester again as a 1:1 mixture of diastereomers. These observations eliminate a dihydride type mechanism and support a pathway shown in Scheme 3 involving heterolytic cleavage of dihydrogen (dideuterium) likely by a nickel carboxylate
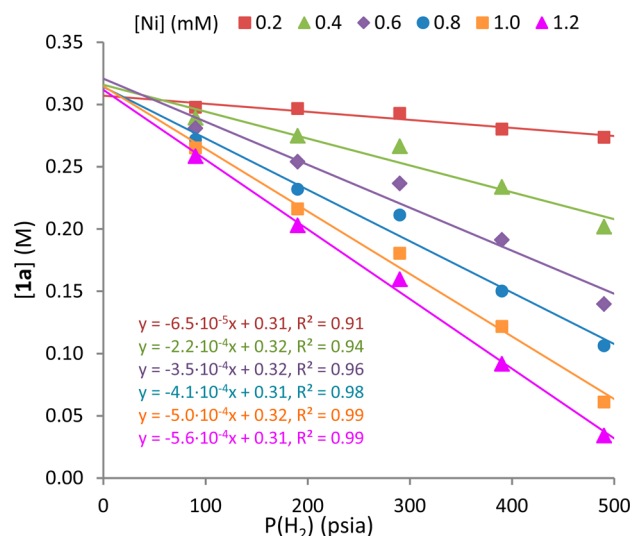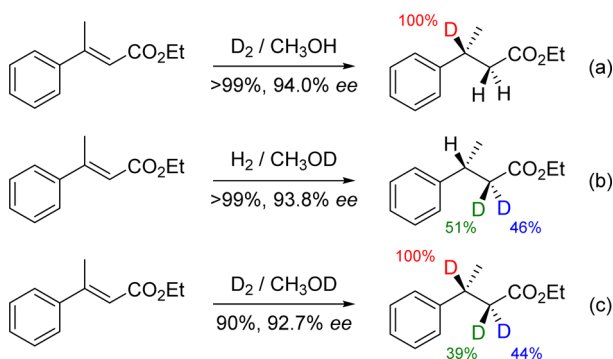
Figure 4. Plot of **1a** remaining vs hydrogen pressure for the asymmetric hydrogenation of **2a**. *Conditions:* 30 μmol (5.7 mg) scale, Ni(OAc)$_2$/(S,S)-Me−DuPhos/Bu$_4$NI (1:1:1), MeOH, 0.3 M, 90−490 psia H$_2$, 50 °C, and 19.25h.

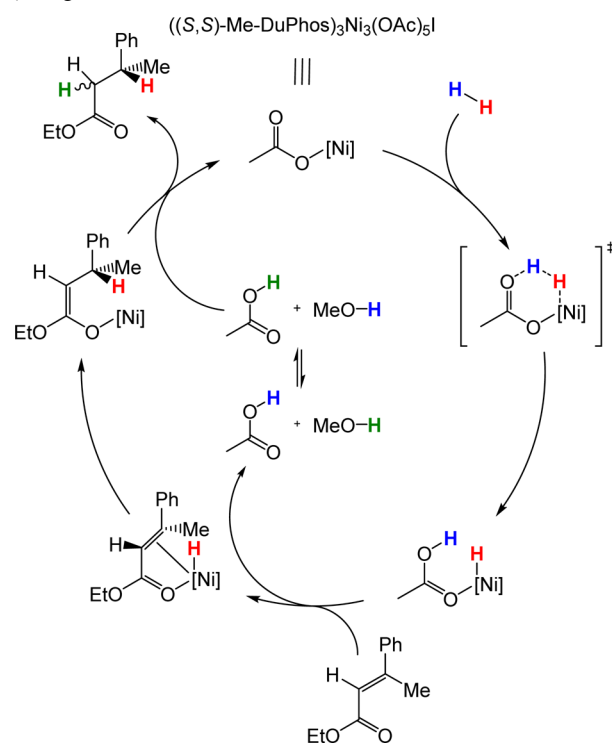**Scheme 2. Deuterium Labeling Studies for the Hydrogenation of 1a by (S,S)-Me−DuPhos Nickel Catalysts in Methanol[a]**

[a]Deuterium incorporation determined by ^{1}H NMR spectroscopy. *Conditions:* 1% Ni(OAc)$_2$, 1.05% (S,S)-Me−DuPhos, 1% Bu$_4$NI, MeOH or MeOD, 0.5M, 500 psi H$_2$ or D$_2$, 50 °C, 18h.

followed by enantioselective conjugate addition of the Ni—H to form a nickel enolate. Subsequent nonselective protonation by methanol releases the alkane.[30] Importantly, these studies establish the critical role of both the nickel carboxylate and the methanol solvent—the former is a key component for the heterolytic activation of dihydrogen while the later is a source of protons for reduction of the alkene. While well established in ruthenium-catalyzed asymmetric hydrogenation, heterolytic H$_2$ cleavage with nickel complexes while precedented,[10b,e,f] is rare and has not been previously applied to asymmetric reductions.

The combined experimental observations are consistent with the pathway shown in Scheme 3. The resting state of the catalyst is the trimeric ((S,S)-Me−DuPhos)$_3$Ni$_3$(OAc)$_5$I complex, which is likely in equilibrium with a number of monomeric and dimeric nickel on complexes on the time scale of catalytic turnover, consistent with coordination chemistry studies and mass spectrometry data. Heterolytic hydrogen activation is rate determining, generating a nickel hydride intermediate and an equivalent of acetic acid.[31] Oxidative addition of dihydrogen to low-valent nickel is unlikely based on

Scheme 3. Proposed Catalytic Cycle for Asymmetric Hydrogenation of 1a

the deuterium labeling studies and the observation that catalysts formed from Ni(COD)$_2$ were unreactive.

CONCLUSIONS

A new nickel catalyst for the asymmetric hydrogenation of α,β-unsaturated esters using H$_2$ as the stoichiometric reductant has been discovered and optimized with the aid of high throughput experimentation. An air stable nickel source in combination with iodide additives and Me−DuPhos were the most effective in methanol solvent and a range of electron donating and withdrawing functional groups were well tolerated. High throughput experimentation also enabled rapid application of the method of continuous variation and kinetic studies and established an unusual trimetallic species, likely formed in low concentration and in equilibrium with other nickel compounds, as the active species for alkene hydrogenation. Deuterium labeling studies identified the essential role of the carboxylate ligands in facilitating the heterolytic cleavage of dihydrogen and the role of methanol as a proton source to complete product formation. These studies have not only validated HTE as a tool for the discovery of new Earth abundant transition metal catalysts for asymmetric hydrogenation, but also demonstrate its utility to rapidly uncover new mechanisms for first row transition metal catalysts and identify active species with unanticipated stoichiometry that evade traditional characterization methods.

ASSOCIATED CONTENT

⑤ Supporting Information

The Supporting Information is available free of charge on the ACS Publications website at DOI: 10.1021/jacs.6b00519.

Characterization data (CIF)
^{1}H and ^{13}C NMR spectra for new compounds and tabulated data from microscale screens (PDF)

■ AUTHOR INFORMATION

Corresponding Authors
*michael_shevlin@merck.com
*pchirik@princeton.edu

Notes
The authors declare no competing financial interest.

■ REFERENCES

(1) New Molecular Entity and New Therapeutic Biological Product Approvals for 2014. See: http://www.fda.gov/Drugs/DevelopmentApprovalProcess/DrugInnovation/ucm429247.htm.

(2) (a) Knowles, W. S. *J. Chem. Educ.* **1986**, *63*, 222−225. (b) Hoge, G. *J. Am. Chem. Soc.* **2003**, *125*, 10219−10227. (c) Hansen, K. B.; Hsiao, Y.; Xu, F.; Rivera, N.; Clausen, A.; Kubryk, M.; Krska, S.; Rosner, T.; Simmons, B.; Balsells, J.; Ikemoto, N.; Sun, Y.; Spindler, F.; Malan, C.; Grabowski, E. J. J.; Armstrong, J. D. *J. Am. Chem. Soc.* **2009**, *131*, 8798−8804.

(3) Blaser, H.-U.; Pugin, B.; Spindler, F.; Thommen, M. *Acc. Chem. Res.* **2007**, *40*, 1240−1250.

(4) Saudan, L. A. *Acc. Chem. Res.* **2007**, *40*, 1309−1319.

(5) Blaser, H.-U.; Malan, C.; Pugin, B.; Spindler, F.; Steiner, H.; Studer, M. *Adv. Synth. Catal.* **2003**, *345*, 103−151.

(6) Shang, G.; Li, W.; Zhang, Z. In *Catalytic Asymmetric Synthesis*, 3rd ed.; Ojima, I., Ed.; John Wiley & Sons: Hoboken, NJ, 2010; Chapter 7, pp 343−436.

(7) (a) Friedfeld, M. R.; Shevlin, M.; Hoyt, J. M.; Krska, S. W.; Tudge, M. T.; Chirik, P. J. *Science* **2013**, *342*, 1076−1080. (b) Monfette, S.; Turner, Z. R.; Semproni, S. P.; Chirik, P. J. *J. Am. Chem. Soc.* **2012**, *134*, 4561−4564.

(8) (a) Sonnenburg, J. F.; Lough, A. J.; Morris, R. H. *Organometallics* **2014**, *33*, 6452−6465. (b) Zuo, W.; Tauer, S.; Prokopchuk, D. E.; Morris, R. H. *Organometallics* **2014**, *33*, 5791−5801. (c) Lagaditis, P. O.; Sues, P. E.; Sonnenberg, J. F.; Wan, K. Y.; Lough, A. J.; Morris, R. H. *J. Am. Chem. Soc.* **2014**, *136*, 1367−1380. (d) Sui-Seng, C.; Freutel, F.; Lough, A. J.; Morris, R. H. *Angew. Chem., Int. Ed.* **2008**, *47*, 940−943.

(9) (a) Sarko, C. R.; DiMare, M.; Yus, M.; Alonso, F. *e-EROS Encyclopedia of Reagents for Organic Synthesis* **2014**, 1−8. (b) Yang, T.-K.; Lee, D.-S.; Haas, J. *e-EROS Encyclopedia of Reagents for Organic Synthesis* **2006**, 1−8.

(10) (a) Angulo, I. M.; Kluwer, A. M.; Bouwman, E. *Chem. Commun.* **1998**, 2689−2690. (b) Angulo, I. M.; Bouwman, E. *J. Mol. Catal. A: Chem.* **2001**, *175*, 65−72. (c) Angulo, I. M.; Bouwman, E.; van Gorkum, R.; Lok, S. M.; Lutz, M.; Spek, A. L. *J. Mol. Catal. A: Chem.* **2003**, *202*, 97−106. (d) Mooibroek, T. J.; Wenker, E. C. M.; Smit, W.; Muitkainen, I.; Lutz, M.; Bouwman, E. *Inorg. Chem.* **2013**, *52*, 8190−8201. (e) Vasudevan, K. V.; Scott, B. L.; Hanson, S. K. *Eur. J. Inorg. Chem.* **2012**, *2012*, 4898−4906. (f) Harman, W.; Peters, J. *J. Am. Chem. Soc.* **2012**, *134*, 5080−5082. (g) Cammarota, R. C.; Lu, C. C. *J. Am. Chem. Soc.* **2015**, *137*, 12486−12489.

(11) For asymmetric hydrogenation of ketones using hydrogen gas, see: (a) Hamada, Y.; Koseki, Y.; Fujii, T.; Maeda, T.; Hibino, T.; Makino, K. *Chem. Commun.* **2008**, 6206−6208. (b) Hibino, T.; Makino, K.; Sugiyama, T.; Hamada, Y. *ChemCatChem* **2009**, *1*, 237−240. For asymmetric transfer hydrogenation of ketones using iPrOH, see: (c) Dong, Z. R.; Li, Y. Y.; Yu, S. L.; Sun, G. S.; Gao, J. X. *Chin. Chem. Lett.* **2012**, *23*, 533−536. (d) Li, Y.-Y.; Yu, S.-L.; Shen, W.-Y.; Gao, J.-X. *Acc. Chem. Res.* **2015**, *48*, 2587−2598.

(12) (a) Yang, P.; Xu, H.; Zhou, J. *Angew. Chem., Int. Ed.* **2014**, *53*, 12210−12213. (b) Guo, S.; Yang, P.; Zhou, J. *Chem. Commun.* **2015**, *51*, 12115−12117. For asymmetric reduction of hydrazones using a similar system, see (c) Xu, H.; Yang, P.; Chuanprasit, P.; Hirao, H.; Zhou, J. *Angew. Chem., Int. Ed.* **2015**, *54*, 5112−5116.

(13) (a) Ghosh, S.; Santulli, R. J.; Kinney, W. A.; DeCorte, B. L.; Liu, L.; Lewis, J. M.; Proost, J. C.; Leo, G. C.; Masucci, J.; Hageman, W. E.; Thompson, A. S.; Chen, I.; Kawahama, R.; Tuman, R. W.; Galemmo, R. A.; Johnson, D. L.; Damiano, B. P.; Maryanoff, B. E. *Bioorg. Med. Chem. Lett.* **2004**, *14*, 5937−5941. (b) Murakami, M.; Kobayashi, K.; Hirai, K. *Chem. Pharm. Bull.* **2000**, *48*, 1567−1569. (c) Baures, P. W.; Eggleston, D. S.; Erhard, K. F.; Cieslinski, L. B.; Torphy, T. J.; Christensen, S. B. *J. Med. Chem.* **1993**, *36*, 3274−3277. (d) Ghorai, P.; Kraus, A.; Birnkammer, T.; Geyer, R.; Bernhardt, G.; Dove, S.; Seifert, R.; Elz, S.; Buschauer, A. *Bioorg. Med. Chem. Lett.* **2010**, *20*, 3173−3176.

(14) Kraft, P.; Bajgrowicz, J. A.; Denis, C.; Fráter, G. *Angew. Chem., Int. Ed.* **2000**, *39*, 2980−3010.

(15) Xu, J.; Ji, F.; Kang, J.; Wang, H.; Li, S.; Jin, D.-Q.; Zhang, Q.; Sun, H.; Guo, Y. *J. Agric. Food Chem.* **2015**, *63*, 5805−5812. (b) Rahman, A. F. M. M.; Angwai, R. F.; Kadi, A. A. *Food Chem.* **2015**, *173*, 489−494.

(16) Rossi, D.; Pedrali, A.; Marra, A.; Pignataro, L.; Schepman, D.; Wünsch, B.; Ye, L.; Leuner, K.; Pevani, M.; Curti, D.; Azzolina, O.; Collina, S. *Chirality* **2013**, *25*, 814−822. (b) Tébéka, I. R. M.; Longato, G. B.; Craviero, M. V.; de Carbalho, J. E.; Ruiz, A. L. T. G.; Silva, L. F. *Chem. - Eur. J.* **2012**, *18*, 16890−16901.

(17) For reviews of high-throughput experimentation techniques, see: (a) Collins, K. D.; Gensch, T.; Glorius, F. *Nat. Chem.* **2014**, *6*, 859−871. (b) Schmink, J. R.; Bellomo, A.; Berrit, S. *Aldrichimica Acta* **2013**, *46*, 71−80. For recent examples of high-throughput experimentation, see: (c) Li, H.; Belyk, K. M.; Yin, J.; Chen, Q.; Hyde, A.; Ji, Y.; Oliver, S.; Tudge, M. T.; Campeau, L.-C.; Campos, K. R. *J. Am. Chem. Soc.* **2015**, *137*, 13728−13731. (d) Buitrago Santantilla, A.; Regalado, E. L.; Pereira, T.; Shevlin, M.; Bateman, K.; Campeau, L.-C.; Schneeweis, J.; Berritt, S.; Shi, Z.-C.; Nantermet, P.; Liu, Y.; Helmy, R.; Welch, C. J.; Vachal, P.; Davies, I. W.; Cernak, T.; Dreher, S. D. *Science* **2015**, *347*, 49−53. (e) Molinaro, C.; Scott, J. P.; Shevlin, M.; Wise, C.; Menard, A.; Gibb, A.; Junker, E. M.; Lieberman, D. *J. Am. Chem. Soc.* **2015**, *137*, 999−1006. (f) DiRocco, D. A.; Dykstra, K.; Krska, S.; Vachal, P.; Conway, D. V.; Tudge, M. *Angew. Chem., Int. Ed.* **2014**, *53*, 4802−4806.

(18) Blaser, H.-U.; Brieden, W.; Pugin, B.; Spindler, F.; Studer, M.; Togni, A. *Top. Catal.* **2002**, *19*, 3−16.

(19) Tang, W.; Wang, W.; Chi, Y.; Zhang, X. *Angew. Chem., Int. Ed.* **2003**, *42*, 3509−3511.

(20) Burk, M. *J. Am. Chem. Soc.* **1991**, *113*, 8518−8519.

(21) See SI Table S1 for complete results of precursor/additive screening.

(22) For a discussion of halide effects in transition metal catalysis, see: Fagnou, K.; Lautens, M. *Angew. Chem., Int. Ed.* **2002**, *41*, 26−47.

(23) Other sources of iodide such as LiI, NaI, and ZnI_2 gave similar results to Bu$_4$NI.

(24) (a) Frenzen, G.; Reim, S.; Sippel, H.; Frauenrath, H. *Z. Kristallogr. - New Cryst. Struct.* **1999**, *214*, 121−122. (b) Frauenrath, H.; Brenthauer, D.; Reim, S.; Maurer, M.; Raabe, G. *Angew. Chem., Int. Ed.* **2001**, *40*, 177−179.

(25) For a review of the method of continuous variation, see: Renny, J. S.; Tomasevich, L. L.; Tallmadge, E. H.; Collum, D. B. *Angew. Chem., Int. Ed.* **2013**, *52*, 11998−12013.

(26) For an example of a multicomponent Job plot, see: Eichhorn, G. L.; Marchand, N. D. *J. Am. Chem. Soc.* **1956**, *78*, 2688−2691.

(27) A multimetallic cluster with a μ_3-iodide ligand is also plausible. Examples of trimetallic nickel clusters with monodentate or small bite angle phosphines are known. For example, see: (a) Morgenstern, D. A.; Wittrig, R. E.; Fanwick, P. E.; Kubiak, C. P. *J. Am. Chem. Soc.* **1993**, *115*, 6470−6471. and (b) Shoshani, M. M.; Johnson, S. A. *Inorg. Chem.* **2015**, *54*, 11977−11985. However, the difference in steric disposition and electronic properties of ^{Me}DuPhos are considerable.

(28) See SI Table S5 for details. For a review of nonlinear effects in asymmetric catalysis, see: Girard, C.; Kagan, H. B. *Angew. Chem., Int. Ed.* **1998**, *37*, 2922−2959.

(29) An observation of first-order rate dependence on nickel concentration is not inconsistent with the trimeric active catalyst species suggested by the Job plot experiments. See (a) Jiang, Y.; Zhang, B.; Li, X.; Wang, X.; Huang, F.; Sun, L. *Angew. Chem., Int. Ed.* **2013**, *52*, 3398−3401. For first order behavior of dimeric ruthenium catalyzed water oxidation (b) Konsler, R. G.; Karl, J.; Jacobsen, E. N. *J. Am. Chem. Soc.* **1998**, *120*, 10780−10781. For first order behavior of dimeric chromium catalyzed asymmetric epoxide opening (c) Anciaux, A. J.; Hubert, A. J.; Noels, A. F.; Petiniot, N.; Teyssié, P. *J. Org. Chem.* **1980**, *45*, 695−702 for first order behavior of dimeric rhodium catalyzed styrene cyclopropanation.

(30) Hydrogenation in the aprotic solvent PhCF$_3$ with D$_2$ gas yielded **2a**-d_2 as the alkane product and the same isotopologue as reaction in MeOD with D$_2$ gas. In the absence of a protic solvent with rapidly exchanging active hydrogen atoms, protonation of the nickel enolate must occur by the acetic acid generated during hydrogen activation.

(31) For a similar carboxylate-mediated hydrogen activation in cobalt-catalyzed carboxylic acid hydrogenation, see: Korstanje, T. J.; van der Vlugt, J. I.; Elsevier, C. J.; de Bruin, B. *Science* **2015**, *350*, 298−302. For a similar carboxylate-mediated hydrogen activation in ruthenium-catalyzed asymmetric hydrogenation of α,β-unsaturated carboxylic acids, see: Ashby, M. T.; Halpern, J. *J. Am. Chem. Soc.* **1991**, *113*, 589−594.